10,03

General boundary conditions for envelope wave functions at semiconductor nanocrystals surface

© K.I. Russkikh, A.V. Rodina

Ioffe Institute,
St. Petersburg, Russia

E-mail: kirill.russkih99@gmail.com

Received October 19, 2023
Revised November 21, 2023
Accepted November 23, 2023

Theoretical calculations of electron energy spectrum and wave functions in spherical semiconductor nanocrystals (NC) surrounded by a dielectric media are presented. The case of high, but finite potential barrier at the NC surface, i.e. at the boundary between semiconductor and dielectric, is considered with account taken for a large difference between electron effective mass inside and outside of NC. We argue that within effective mass method such NC surface can be described as impenetrable for electron with nonvanishing envelope wave functions at the boundary. General boundary conditions that provide a consistent description of quantum size energy levels of localized electron states are suggested and the conditions of their applicability are determined. General boundary conditions are characterized by a single surface parameter that depends only on the height U of the potential barrier and electron effective mass m_B outside NC. We show that the energies of electron levels decrease while the probability of finding electron at the NC surface increases with increasing m_B. The analytical asymptotic expressions for the dependence of the electron ground state energy on U and m_B are obtained.

Keywords: semiconductors, quantum dots, nanocrystals, boundary conditions, effective mass method.

DOI: 10.21883/0000000000

1. Introduction

Semiconductor nanocrystals (NC) also known as colloidal quantum dots became the first low-dimensional semiconductor nanosystem that ensures spatial confinement of charge carriers in all three directions [1]. Size quantization spectra in zero-dimensional structures were first studied for CuCl nanocrystals in a glass matrix [2] and for CdS nanocrystals in aqueous solution [3]. Theory of absorption spectra of spherical NC in various size quantization conditions was developed in [4]. Semiconductor NC are now one of the best investigated low-dimensional semiconductor nanosystems [1]. High quantum yield and controlled changing of optical transition energy by the size variation make the colloidal semiconductor NC highly demanded in a wide application range [5]: new lasers [6], various optoelectronic devices [7], quantum computer qubits [8,9]. Semiconductor NC are widely used for biological [10] and medical [11] purposes.

Many NC applications are associated with the surface functionalization ability. Modern chemical synthesis makes it possible to control surface passivation with organic molecules (ligands) and to replace ligands after synthesis completion. Experiments show that replacement of ligands on the NC surface results in variation of optical transition energies and other observed properties [12]. This creates a need in a theoretical model to consider the dependence of electronic states localized inside NC not only on the semiconductor material properties, but also on the surrounding dielectric medium and NC surface conditions. Using numerical calculations within the density functional theory (DFT) as well as the effective mass method analysis, [13] reported that the length of electron tunneling from two-dimensional nanoplatelets or spherical nanocrystals into the organic shell is almost completely determined by ligand properties.

The effective mass approximation is one of the first theoretical methods in research of semiconductor heterostructures [14,15] and nanocrystals [3,4] with abrupt boundaries. Advantage of this method compared with more accurate numerical methods is in effective theoretical modelling and analysis of physical phenomena. However, application of the effective mass method to the abrupt bounded structures requires proper solution of the issue of boundary conditions at interfaces. Full wave function representation as an expansion in basic Bloch functions for one or more energy bands is only possible in the structure material to the left and right of the boundary where envelope wave functions (expansion coefficients) and effective Hamiltonian parameters $\hat{H}$ are determined. Therefore, to apply the effective mass method to abrupt bounded structures, boundary conditions (BC) shall be formulated for envelope wave functions. Such boundary conditions shall ensure self-adjointness of $\hat{H}$ that is equivalent to the continuity of normal component of the probability flow density vector across the boundary $J_n = (\hat{\mathbf{J}} \cdot \mathbf{n})$, where $\mathbf{n}$ is the unit normal vector to the boundary surface [16].

For one-band effective mass method in case of finite potential barrier (e.g. in case of the planar heterostructure [14,15] or core/shell type spherical system [17]), the

standard boundary conditions (SBC) stipulate continuity of the wave function Ψ and Ψ'/m_e, where $'$ is a derivative in direction $\mathbf{n}$, m_e is the electron effective mass. Such SBC are a special case of general boundary conditions (GBC) assigned using the interface matrix [18]. For the multiband effective mass method, the similar result was achieved in [16]. It is essential that SBC are not always applicable to the multiband method. For example, this is the case when the Bloch functions vary widely in various materials [19] or do not exist in the boundary region [20]. Also, SBC prevent from describing interface effects, e.g. boundary-induced mixing of states with various symmetries [21–24].

The surface of semiconductor NC surrounded with dielectric matrix or organic medium, like the semiconductor/vacuum interface, is often treated as a high impenetrable barrier for electrons. This corresponds the boundary condition $J_n = 0$. Within the one-band method, the impenetrability condition may be easily fulfilled with the Dirichlet boundary condition $\Psi = 0$ [4]. However, such BC prevent from considering the surface properties that may affect the electron spectrum even in case of high potential barrier. For example, [25,26] used SBC to consider the influence of the effective electron mass jump, i.e. the difference of m_e to the left and to the right of the semiconductor/vacuum interface. The effect of mass jump on the energy of two lower electron levels in spherical NC with finite potential barrier height was studied in [27], whilst the inside effective electron mass was fixed and the outside mass was varied. SBC or GBC, considering the finite, though high barrier for semiconductor NC surface, are used in the cases when outflow of the electron wave function into the matrix shall be explicitly considered (e.g. when calculating the nonradiative Auger recombination rate [28] or transport properties of the nanocrystal array [29]). Even in case of high potential barrier, the envelope electron wave function at the semiconductor interface has a non-zero value which is important for description of many effects caused by the NC surface. For example, such effects include the surface effect on light absorption in indirect band gap semiconductor NC [30], exchange interaction between an electron and dangling bonds on the NC surface [31], surface-induced spin-orbit interaction and surface contribution to the electronic magnetic moment [32] localized at the Tamm state surface.

It should be noted that in case of high potential barrier at the semiconductor/dielectric interface, SBC may forecast envelope wave function decay in the barrier at distances less than of the order of the lattice constant. Since the effective mass method involves slow variation of envelope wave functions on the lattice cell scale, then they shall be assumed equal to zero outside NC and the barrier shall be treated as impenetrable. However, the flow disappearance condition $J_n = 0$ for an impenetrable barrier does not require vanishing of the envelope wave function at the NC interface. General boundary conditions for the impenetrable potential barrier that contain a surface parameter in addition to volumetric parameters $\hat{H}$ were offered in [16,32]. This parameter has a length dimension and characterizes the near-surface layer width where the envelope wave functions are not well defined. Such GBC may be also used when there is a localizing short-range potential near the surface where surface Tamm states may exist [16,32]. In [32,33], surface parameter value was determined for CdSe NC by means of analysis of experimentally measured dependence of effective g-factor of the electron on the NC diameter. However, the application conditions of GBC offered in [16,32] for the impenetrable potential barrier and connection between the surface barrier, potential barrier value and effective electron mass in the surrounding medium were not studied.

Te purpose of the study is to perform theoretical analysis and comparison of electron size quantization spectra in spherical NC with high potential barrier that are calculated within a one-band effective mass model using both GBC for the impenetrable barrier and SBC for the finite barrier. Such comparison makes it possible to define the connection between the GBC surface parameter, potential barrier height and effective electron mass in the surrounding matrix, and the GBC applicability region.

2. Problem formulation

The Schrödinger equation $\hat{H}\Psi = E\Psi$ for electron states in spherical nanocrystals after substitution of wave functions as $\Psi(\mathbf{r}) = R_l(r)Y_{l,m}(\theta, \phi)$, where $Y_{l,m}$ are spherical harmonics (l is the orbital moment and m is the magnetic quantum number), becomes one-dimensional.

$$-\frac{1}{r^2}\frac{\mathrm{d}}{\mathrm{d}r}\left(r^2\frac{\mathrm{d}R_l(r)}{\mathrm{d}r}\right) + \frac{R_l(r)}{r^2}\,l(l+1) - \frac{2m_e(r)}{\hbar^2}\,(V(r) - E)R_l(r) = 0. \qquad (1)$$

Here, $V(r)$ and $m_e(r)$ describe the dependence of potential energy and electron mass on distance r from NC center with radius a:

$$V(r) = \begin{cases} U & r > a \\ 0 & r \le a \end{cases}, \quad m_e(r) = \begin{cases} m_B & r > a \\ m_A & r \le a. \end{cases} \qquad (2)$$

Whilst the radial component of the wave function $R_l(r)$ may be also represented as a piece continuous function

$$R_l(r) = \begin{cases} R_l^B(r) & r > a \\ R_l^A(r) & r \le a \end{cases} \qquad (3)$$

and is subject to normalization condition

$$\int_0^a r^2 dr |R_l^A(r)|^2 + \int_a^\infty r^2 dr |R_l^B(r)|^2 = P_l^A + P_l^B = 1. \qquad (4)$$

P_l^A and P_l^B values are probabilities of finding an electron inside and outside NC, respectively.

Standard BC $R_l^A(a) = 0$ in the infinitely high potential barrier model $U \to \infty$ give the following expression for the electron energy spectrum

$$E_{l,n}^{\infty} = \frac{\hbar^2 \gamma_{l,n}^2}{2m_A a^2} = \frac{\gamma_{l,n}^2}{\pi^2} E_q, \quad E_q = \frac{\hbar^2 \pi^2}{2m_A a^2}. \tag{5}$$

where $\gamma_{l,n}$ is the n-th root of the l-the order spherical Bessel function. To study the effect of the difference of effective electron masses m_A and m_B inside and outside NC with an arbitrary potential barrier height U, electron energies $E_{l,n}$ and radial wave functions $R_{l,n}(r)$ will be calculated for four lower size quantization levels with $l = 0\,(n = 1, 2)$, $l = 1\,(n = 1)$ and $l = 2\,(n = 1)$ using standard boundary conditions.

$$R_l^A(r)\big|_{r=a} = R_l^B(r)\big|_{r=a}, \quad \frac{1}{m_A}\frac{\mathrm{d}R_l^A}{\mathrm{d}r}\Big|_{r=a} = \frac{1}{m_B}\frac{\mathrm{d}R_l^B}{\mathrm{d}r}\Big|_{r=a}. \tag{6}$$

Special focus will be made to the spectra variation with an increase in relative barrier height U/E_q and a decrease in effective mass ratio inside and outside NC $\mu = m_A/m_B$.

For the impenetrable potential barrier corresponding to the range of values $U/E_q \gg 1$, we will consider the general boundary conditions offered in [16,32] in a restated form

$$R_l^A(r)\big|_{r=a} = -\frac{m_B}{m_A} A \frac{\mathrm{d}R_l^A}{\mathrm{d}r}\Big|_{r=a}, \quad R_l^B(r > a) = 0. \tag{7}$$

Here, A is the parameter that has a length dimension and does not depend on a, l and n. Comparison of spectra and wave functions calculated using SBC (6) and GBC (7) will allow the connection between A and potential barrier parameters U and m_B to be found and the GBC applicability region (7) to be determined to describe size-quantized electron states in NC with the impenetrable barrier.

3. Energy spectrum and wave functions with SBC

3.1. Energy level equations

Wave functions corresponding to the solution of equation (1) are written as

$$R_l^A(r) = C_l 2k_l j_l(k_l r), \quad R_l^B(r) = C_l \mathscr{B}_l \varkappa_l h_l^{(1)}(i\varkappa_l r), \tag{8}$$

where wave numbers k_l and $\varkappa_l$ are related to the level energy E_l as

$$E_l = \frac{\hbar^2 k_l^2}{2m_A}, \quad U - E_l = \frac{\hbar^2 \varkappa_l^2}{2m_B}, \tag{9}$$

$j_l(k_l r)$ and $h_l^{(1)}(i\varkappa_l r)$ are spherical Bessel and Hankel functions, respectively [34]. C_l is defined by normalization condition (4). Substituting wave functions (8) into the first BC from (6) gives the following constant

$$\mathscr{B}_l = \frac{2k_l j_l(k_l a)}{\varkappa_l h_l^{(1)}(i\varkappa_l a)}, \tag{10}$$

and substituting (8) and (10) into the second BC from (6) reduces to equations for energy level calculation

$$l = 0: \quad \tan(k_0 a) = \frac{k_0 a}{1 - \mu(1 + \varkappa_0 a)} \equiv F_0(k_0 a, \varkappa_0 a, \mu),$$

$$l = 1, 2: \ \tan(k_l a) = F_l(k_l a, \varkappa_l a, \mu). \tag{11}$$

Explicit expressions for $F_l(k_l a, \varkappa_l a, \mu)$ for $l = 1, 2$ are given in Appendix 1A. For simplification of the formula, the quantum number n that defines the level number with assigned value l is omitted in the equations above.

3.2. Dependence of energy levels on the barrier height and effective mass ratio

Calculation of $E_{l,1}$ s-, p- and d-symmetry energy levels ($l = 0, 1, 2$) with SBC according to the potential barrier height U in terms of E_q are shown in Figure 1, *a*. As shown in the figure, with decreasing mass ratio $\mu = m_A/m_B$, E_l values increasingly deviate from asymptotic values E_l^{∞} that satisfy $U \to \infty$. Energy levels are limited by dot-and-dash line $E_l = U$ to the right of which there are no localized electron states of this symmetry with energy below the potential barrier. It is convenient to express critical heights of the localizing potential barrier for each level as a condition on the quantum well power $\mathrm{w}_u \le \mathrm{w}_{l,n}$, where

$$\mathrm{w}_u = a\sqrt{\frac{2m_A U}{\hbar^2}} = k_u a. \tag{12}$$

Critical values of $\mathrm{w}_{l,n}$ are obtained from equations

$$l = 0: \quad \mathrm{w}_{0,n}\cot(\mathrm{w}_{l,n}) = 1 - \mu \equiv W_0(\mu),$$

$$l = 1, 2: \ \mathrm{w}_{l,n}\cot(\mathrm{w}_{l,n}) = W_l(\mu, \mathrm{w}_{l,n}), \tag{13}$$

that are derived from (11) when substituting $k_{l,n} = k_u$ and $\varkappa_l = 0$ for $E_{l,n} = U$. Explicit expressions for $W_l(\mu, \mathrm{w}_{l,n})$ for $l = 1, 2$ are given in Appendix 2A.

Figure 1, *b* shows dependence $\mathrm{w}_{l,n}$ on the mass ratio μ. For $\mu = 1$, delocalization of s-symmetry levels takes place when the spherical quantum well power is lower than $\mathrm{w}_{0,n} = \pi(n - 1/2)$. For ground state $n = 1$, this condition coincides with the known condition for the critical depth of 3D-potential that allows electronic localization at U higher than $U^{\mathrm{cr}} = E_q/4$. However, the high effective electron mass in the matrix compared with the electron mass in the semiconductor ($\mu < 1$) allows electronic localization in the NC core at lower $\mathrm{w}_{0,n} < \pi(n - 1/2)$. Delocalization of electron with orbital moments $l = 1, 2$ for $\mu = 1$ occurs at $\mathrm{w}_{l,n} = \gamma_{l-1,n}$. With decreasing μ, critical well powers also decrease.

Figure 2 shows the energy spectrum variation (energies of four lower electron levels in terms of E_q) from the effective mass ratio μ at fixed dimensionless potential $U/E_q = 20$ (Figure 2, *a*) and at fixed dimensionless potential $U/E_q^B = 200$ (Figure 2, *b*), where $E_q^B = \mu E_q$. The calculated dependences are invariant to the method of

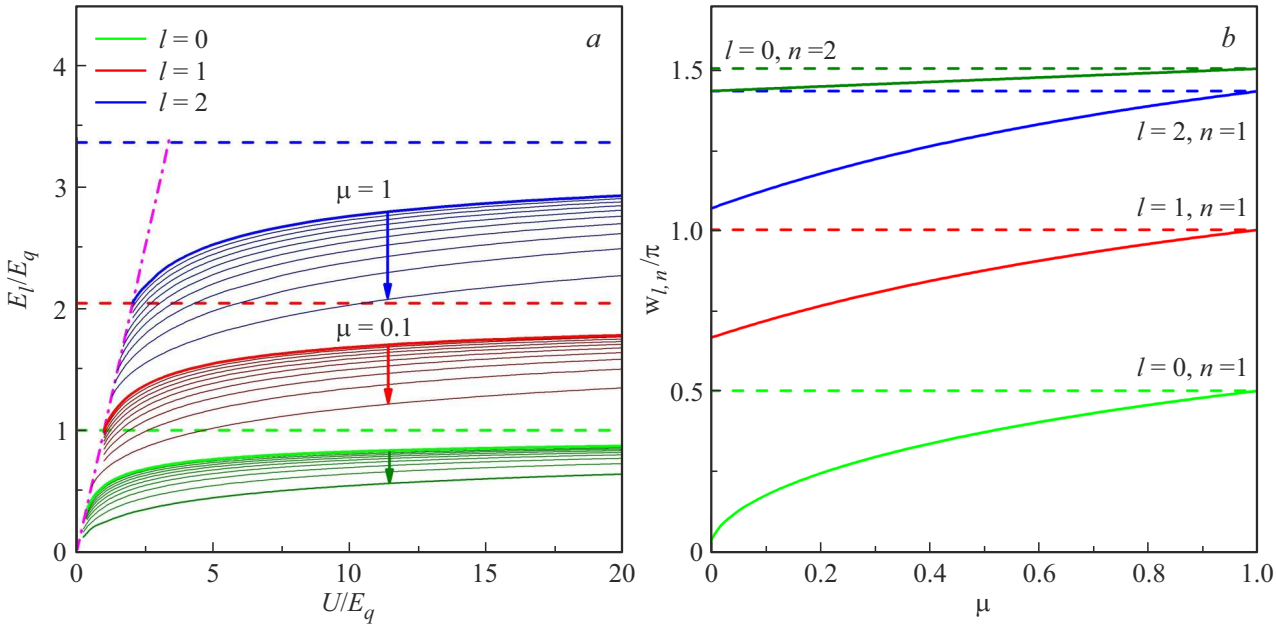

Figure 1. (a) Dependence of $E_{l,1}$ on U with various μ values for orbital moments $l = 0, 1, 2$ with SBC (6). Horizontal dashed lines correspond to asymptotic energy values $E^{\infty}_{l,n}$. Energies are expressed in terms of E_q. (b) Dependence of critical values of spherical quantum well powers $w_{l,1}$ ($l = 0, 1, 2$) and $w_{0,2}$ on the effective mass ratio μ. Horizontal dashed lines correspond to asymptotic energy values at $\mu = 1$.

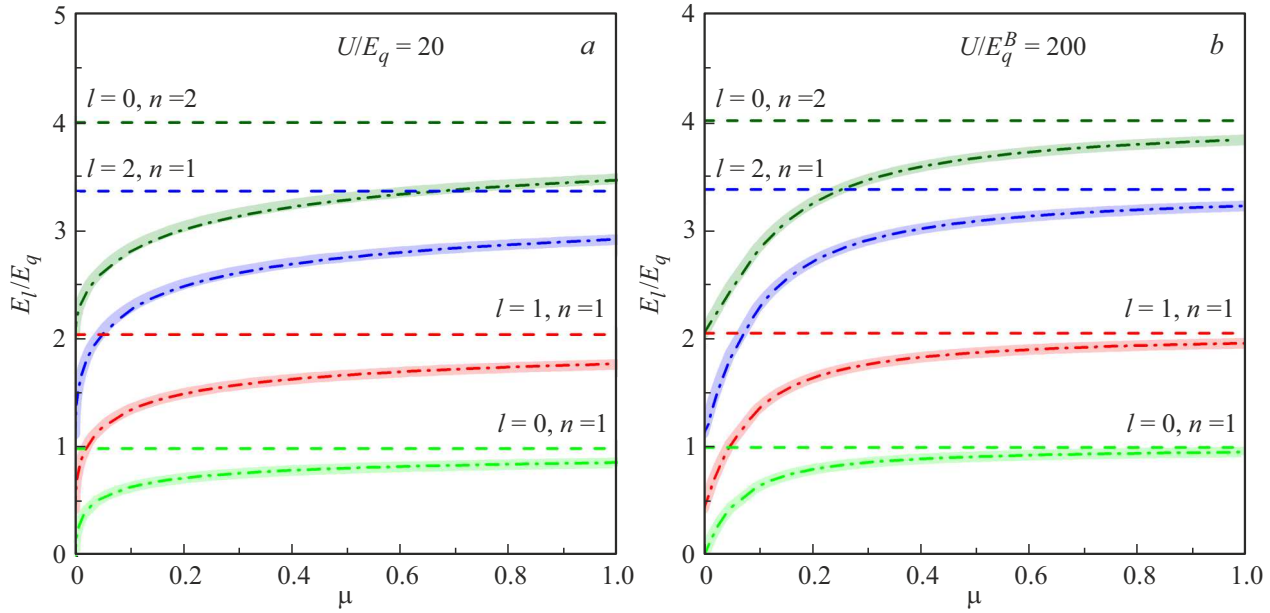

Figure 2. Energy spectrum evolution depending on mass ratio μ in universal coordinates that give similar energies for two mass variation methods. Energies are measured in terms of E_q, dimensionless potential height is fixed as $U/E_q = 20$ and $U/E_q^B = 200$ ($E_q^B = \mu E_q$) in panes (a) and (b), respectively. Horizontal dashed lines correspond to asymptotic energy values $E^{\infty}_{l,n}$. The energy spectrum was calculated with SBC (6) (dot-and-dash lines) and GBC (7) (thick solid lines).

μ variation, i. e. increase of the m_B or decrease of the m_A. $\mu = 1$ in panel (b) corresponds to a higher potential $U/E_q = U/E_q^B = 200$ than in panel (a), which causes higher electron energies. It should be noted that, though dimensionless energy $E_{l,n}/E_q$ in terms of E_q always decreases with a decrease in μ, behavior of the absolute level energy dependence $E_{l,n}$ varies depending on the varied mass. Thus, at fixed mass m_A inside NC and increase in $m_B/m_0 \to +\infty$, where m_0 is the free electron mass, absolute energies $E_{l,n}$ decrease. However, the absolute

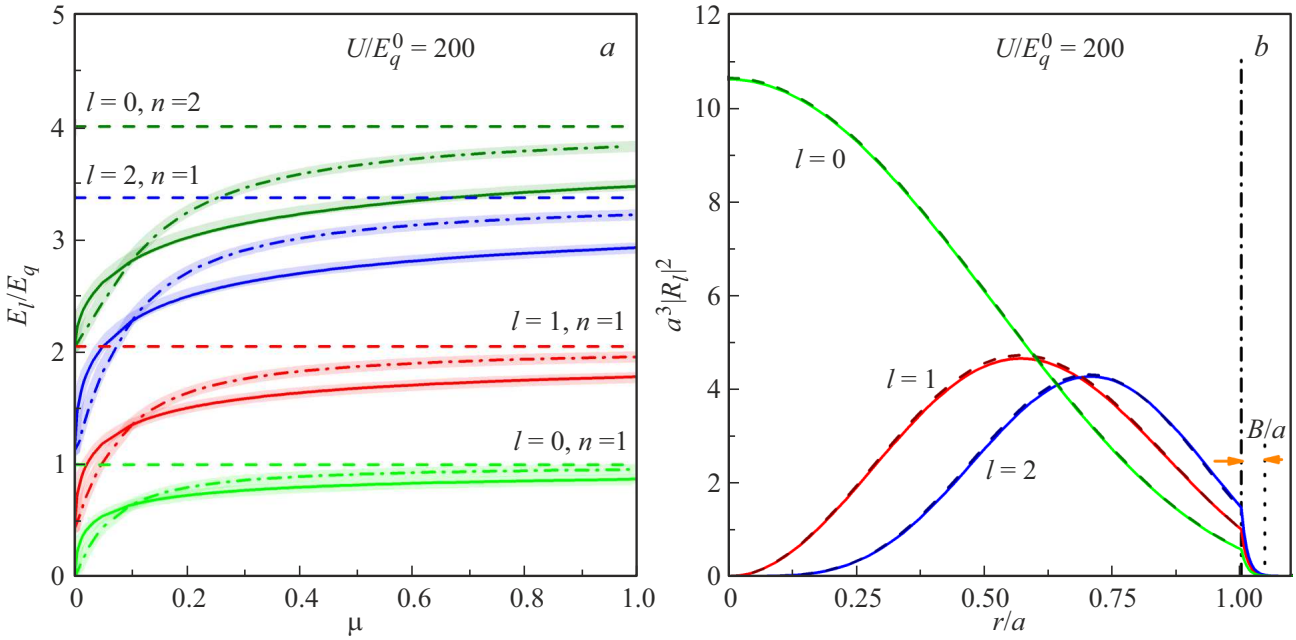

Figure 3. (a) Energy spectrum evolution for two methods of μ variation: variation of m_A inside NC at fixed $m_B = m_0$ (dot-and-dash lines) and variation of m_B outside NC at fixed $m_A = 0.1m_0$ (solid lines). The calculation was performed at fixed potential barrier height $U/E_q^0 = 200$ using SBC (6) (thin lines) and GBC (7) (thick lines); horizontal dashed lines correspond to asymptotic energies $E_{l,n}^{\infty}$. (b) Dependences of the dimensionless density of probability of finding an electron at distance$r$ from the center of NC with radius a for three levels$l = 0, 1, 2$ ($n = 1$) calculated with SBC (6) (solid lines) and GBC (7) (dashed lines) in case of high potential barrier $U/E_q^0 = 200$ and effective masses $m_A = 0.1m_0$ and $m_B = m_0$ ($\mu = 0.1$).

potential barrier height U in Figure 2, a remains constant and decreases in Figure 2, b. On the contrary, at fixed m_B and $m_A/m_0 \to 0$, energies $E_{l,n}$ grow, though slower than E_q. As will be shown below, for the ground state $l = 0$, $E_{0,0}$ always has a finite value at $m_A/m_0 \to 0$ and is defined by mass m_B.

It is interesting also to follow the impact of the effective electron mass difference on the energy level position relative to the constant potential barrier U which is independent on the effective masses inside NC and in the dielectric medium. Figure 3, a shows dependences of the energy spectrum on the mass ratio at the fixed potential barrier $U/E_q^0 = 200$ (where $E_q^0 = E_q m_A/m_0$) for two variation methods $\mu = m_A/m_B$. For fixed $m_A = 0.1m_0$, spectrum behavior with increasing m_B coincides with that shown in Figure 2, a. At the same time, for fixed $m_B = m_0$, spectrum behavior with decreasing m_A coincides with that shown in Figure 2, b. It is shown that at fixed potential barrier U/E_q^0, energies are different at the same mass ratio μ implemented at different m_A and m_B values. For example, $\mu = 1$ in Figure 3, a is implemented at $m_A = m_B = 0.1m_0$ and $m_A = m_B = m_0$. However, an increase in mass outside NC results in a decrease in level energy $E_{l,n}$ relative to the barrier height, and a decrease in mass m_A inside NC results in an increase. $\mu = 0.1$ is implemented at $m_A = 0.1m_0$ and $m_B = m_0$ (the situation typical for the semiconductor/vacuum or semiconductor/dielectric interface), whilst deviations of $E_{l,n}$ from asymptotic $E_{l,n}^{\infty}$ for the potential barrier are considerable and may not be considered any longer as small corrections within the perturbation theory.

3.3. Probability of electron detection on the NC surface and outside NC

The effect of potential barrier parameters on the radial electron wave function behavior $R_l(r)$ is described below. Figure 3, b shows the distribution of the dimensionless probability density $a^3|R_l(r)|^2$ at $U/E_q^0 = 200$ and $m_A = 0.1m_0$, $m_B = m_0$ ($\mu = 0.1$). The typical tunneling length of the wave function beyond the NC boundaries may be estimated as $\approx 1/\varkappa_{l,n}$. However, as shown in (9) [see also Figure 3, b], with high potential barrier $U \gg E_{l,n}$, this length is much the same for all described levels and is equal to the effective length B that depends only on external parameters, i. e. the mass inside the potential barrier m_B and the potential barrier height U:

$$B = \sqrt{\frac{\hbar^2}{2m_B U}}. \qquad (14)$$

For the high potential barrier and large effective electron mass outside NC, B is of the order of the lattice constant. In this case, description using envelope wave functions outside NC is, strictly speaking, not applicable. For the wave functions shown in Figure 3, b, for example, $B/a \approx 0.0225$. For NC with a diameter of 5 nm, this

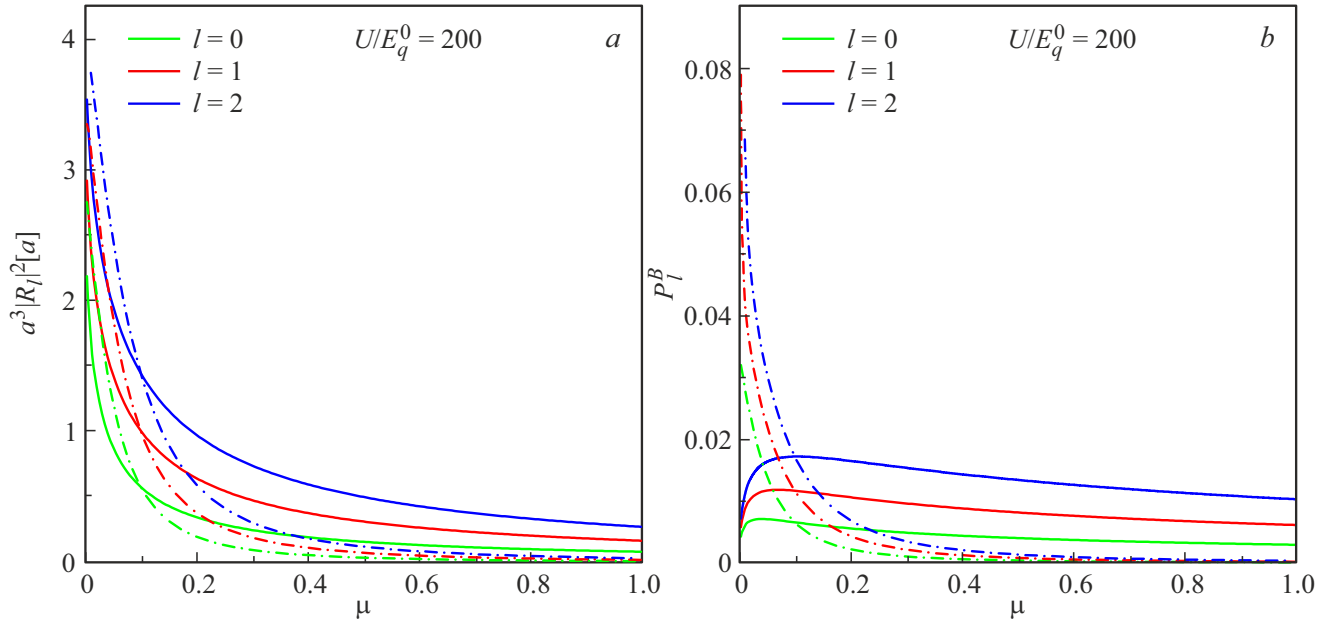

Figure 4. Dependence (a) of the dimensionless electron density $a^3|R_l(r=a)|^2$ at the NC boundary and (b) electron localization probability P_l^B outside NC on μ: with variation of m_A inside NC at fixed $m_B = m_0$ (dot-and-dash line) and for mass variation outside NC m_B at fixed $m_A = 0.1m_0$ (solid line). The calculation uses the fixed potential barrier height $U/E_q^0 = 200$ for three levels $l = 0, 1, 2$ ($n = 1$).

corresponds to $B \approx 0.06$ nm. Such order of the tunneling length is typical for NC surrounded with ligands. As shown in [13], the tunneling length from CdSe nanoplatelets to the organic ligand shell does not exceed 0.15 nm at the effective mass in the shell $m_B = 1.255m_0$ ($\mu \approx 0.1$) and potential barrier height U of the order of 1–2 eV. The wave function overlap integral between two nanocrystals decreases with increasing distance between them with the typical length $\approx 1/2\varkappa_{l,n} \approx B/2$ in the limiting case of high potential barrier [13]. High potential barriers of the order of 10 eV may be formed in case of surface passivation with alkane chain type organic compounds [35].

However, it should be noted that the boundary condition of envelope wave function vanishing at the NC boundary in model $U \to \infty$ is also not applicable to small μ. Actually, Figure 3, b clearly shows that the dimensionless probability density $a^3|R_l(a)|^2$ for electron detection at $r = a$, in particular for excited states, is comparable with the values inside NC for $\mu = 0.1$. Dependence $a^3|R_l(r=a)|^2$ on μ at constant $U/E_q^0 = 200$ for two methods of μ variation is shown in Figure 4, a.

We consider the electron detection probability variation

$$P_l^B = \int_a^\infty r^2 dr |R_l^B(r)|^2$$

outside NC shown in Figure 4, b for two variation methods of μ. In case of a constant mass $m_A = 0.1m_0$ inside NC, the probability P_l^B initially grows a little with increasing m_B from 0.1 m_0 to m_0, and then drops significantly with further growth of the mass outside the barrier. Nonmonotonical dependence is caused by the competition of two factors — probability density growth at the NC boundary and simultaneous decrease of the outflow length B with increasing m_B. In the second case of constant mass m_B, probability of electron tunneling beyond the NC boundary grows with decreasing m_A. Whilst for the parameters at which the energy level localization conditions $E_l < U$ are met, $P_l^B < 0.08$.

4. Results: Energy spectrum and wave functions when with GBC

4.1. Determining the surface parameter and GBC applicability region

Consider the reproducibility of results obtained with SBC (6) for the high potential barrier case with GBC (7). First, estimate A in equation (7) using $E_{l,n}$ found with SBC and substituting $k_{l,n}$ values corresponding to them into the wave functions $R_l(r)$ determined inside NC at $r = a$. For each energy level, find $A_{l,n}$ from (7) as

$$A_{l,n} = -\mu \frac{R_l^A(a)}{R_l^{A'}(a)} = \frac{m_A}{m_B} \frac{j_l(k_{l,n}a)}{k_{l,n}[j_{l-1}(k_{l,n}a) - j_l(k_{l,n}a)(l+1)/(k_{l,n}a)]}, \quad (15)$$

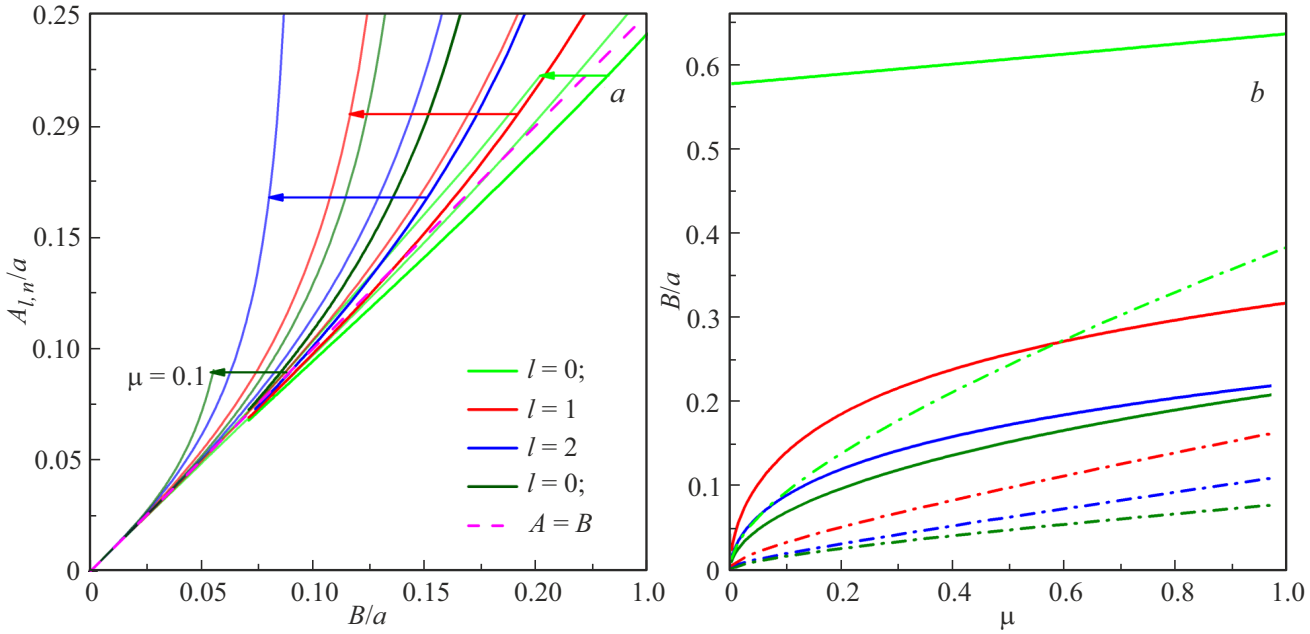

Figure 5. (a) Dependence of the dimensionless GBC parameter $A_{l,n}/a$ on B/a for four lower electron levels at various μ values. Dashed line shows the linear dependence $A/a = B/a$. (b) — GBC applicability region with $A = B$ on the B/a and μ plane: solid lines — dependences $B^{\rm cr}_{l,n}(\mu)$ that set prerequisite $B/a < B^{\rm cr}_{l,n}$ for electron state localization; dot-and-dash lines — dependences $B_{l,n}(\mu)$ according to approximations $B_{0,1} = 0.250\sqrt{\mu} + 0.133\mu + 0.002$, $B_{1,1} = 0.067\sqrt{\mu} + 0.097\mu + 0.004$, $B_{2,1}/a = 0.026\sqrt{\mu} + 0.082\mu + 0.005$ and $B_{0,2}/a = 0.042\sqrt{\mu} + 0.037\mu + 0.001$ that set sufficient condition $B/a \le B_{l,n}(\mu)/a$ for description of electron states with accuracy at least 6%.

where $'$ means the spatial derivative. For $U/E^0_q = 200$, $m_A = 0.1m_0$ and $m_B = m_0$, we obtain

$$A_{0,1}/a = 0.0223; \quad A_{1,1}/a = 0.0227;$$

$$A_{2,1}/a = 0.0233; \quad A_{0,2}/a = 0.0237.$$

Thus, $A_{l,n}/a \approx A/a \approx B/a$ for all described electron states.

Condition $A_{l,n}/a \approx A/a \approx B/a$ may be considered as a sufficient condition for finding the spectrum and electron wave functions for states with quantum numbers $l' = 0, 1, \ldots l$, $n' = 1, \ldots n$ when using GBC (7) with surface parameter $A = B$. The existence of localized states $E_{l,n} < U$ is the prerequisite. This condition is satisfied for $B/a < B^{\rm cr}_{l,n}/a = \sqrt{\mu}/{\rm w}_{l,n}$, where ${\rm w}_{l,n}$ are critical quantum well powers [see Figure 1, b]. Fulfilment of the level localization prerequisite makes it possible to neglect the probability of finding an electron outside NC that, as shown in Figure 4, a, increases at low μ.

Now consider dependences of $A_{l,n}/a$ on B/a as shown in Figure 5, a for four lower electron levels found with SBC. It is shown that when μ decreases, the region of coincidence of all $A_{l,n}/a \approx A/a = B/a$ is also changed, i. e. the region of sufficient condition for GBC application. However, this region is always inside the region of $B/a < B^{\rm cr}_{l,n}/a$ that is responsible for the level localization prerequisite. Assume the region of $B/a \le B_{l,n}/a$ as the GBC applicability region, when all $A_{l,n}$ values at specified μ deviate from B/a by max. 6%. In Figure 5, b, dot-and-dash lines show the calculated approximations for dependences of $B_{l,n}/a$ on μ describing the GBC applicability region for the spectrum from lower s, p and d levels $l = 0, 1, 2$, ($B_{l,1}$) and including the excited s level $l = 0, n = 2$ ($B_{0,2}$). Solid lines show dependences of $B^{\rm cr}_{l,n}/a$ on μ.

4.2. Energy level equations

Now derive the equations for electron energy calculation with GBC (7). Wave functions are written as (8), where $\mathscr{B}_l = 0$, and C_l is found from normalization condition (7) that reduces to $P^A_l = 1$.

Equations for determining energy levels with GBC (7) are written as

$$l = 0: \quad \tan(k_0 a) = k_0 a \frac{A}{A - \mu a} \equiv f_0(k_0 a, \tilde{A}),$$

$$l = 1, 2: \ \tan(k_l a) = f_l(k_l a, \tilde{A}), \quad \tilde{A} = \frac{A}{a}\frac{1}{\mu}. \qquad (16)$$

Explicit form of f_l is shown in Appendix 1A. Limiting transition $E_{l,n} \to E^{\infty}_{l,n}$ at $\tilde{A} \to 0$ obviously takes place. Level energies $E_{l,n}$ found using GBC (7) with $A = B$ coincide with those found earlier using SBC with accuracy at least 6% provided that $B/a \le B_{l,n}/a$. Dependence of four lower energy levels on μ for $U/E_q = 20$, $U/E^B_q = 200$ and $U/E^0_q = 200$ are shown by light thick lines in Figure 3, a, respectively. Wave function found with GBC for $U/E^0_q = 200$, $m_A = 0.1m_0$, $m_B = m_0$ are shown by dark dashed lines in Figure 3, b.

5. Discussion of results: effect of the impenetrable NC surface on the electron energy spectrum

Thus, comparison of energies and wave functions for four electron states found with SBC (6) and GBC (7) made it possible to define the potential barrier parameter region where the barrier may be represented as impermeable. The only GBC surface parameter contains the details of the barrier parameters: potential barrier height and effective electron mass outside NC. Therefore the effect of the dielectric medium that surrounds NC on the energy levels may be described even in the impenetrable potential barrier model. Though the size quantization energies are primarily defined by the electron mass m_A inside NC, an increase in the electron mass m_B in the dielectric medium results in decrease in the electron energy levels. On the other side, the energy levels increase slower with decreasing m_A than $E_l^\infty \propto 1/m_A$, because the dimensionless energies $E_{l,n}/E_q$ decrease with decreasing $\mu = m_A/m_B$.

The obtained analytical expressions for the energy spectrum with GBC are simpler than in case of SBC and make it possible to find analytical asymptotic behavior of the energy levels in limiting cases. $\mu \to 0$ case corresponds to $\tilde{A} \to +\infty$ case at $A/a \neq 0$ and may be considered for small surface parameter values satisfying $A/a < B_{l,n}(\mu)/a$ [see Figure 5, *b*]. In this case, for symmetry levels *s*-, we obtain

$$\lim_{\tilde{A}\to+\infty} f_0(k_0 a, \tilde{A}) = k_0 a. \qquad (17)$$

Asymptotic expressions for f_l are given in Appendix 1A. Dimensionless excited state energies $E_{0,2}/E_q = E_{1,1}^\infty/E_q \approx 2.046$, $E_{1,1}/E_q \approx 0.439$ and $E_{2,1}/E_q \approx 1.132$ have their finite values at $\mu \to 0$. Though E_q goes to infinity at $m_A/m_0 \to 0$, excited state energy levels are always below the potential barrier U.

The electron ground state is described in more detail below. Within $\mu \to 0$, the dimensionless energy $E_{0,1}/E_q \to 0$. Show that the absolute energy within this boundary remains non-zero and the order of levels with orbital moment $l = 0, 1, 2$ is maintained. By expanding the left-hand side of equation (16) into the Taylor's series in a small parameter $k_0 a$ near point $\mu = 0$ and the right-hand side in a small parameter $1/\tilde{A} = \mu a/A$, we obtain the energy expression

$$\frac{E_{0,1}}{E_q} \approx \frac{3}{\pi^2}\frac{1}{\tilde{A}} \Rightarrow E_{0,1} \approx 3\sqrt{\frac{\hbar^2 U}{2m_B a^2}}. \qquad (18)$$

Expression (18) shows that the ground state energy $E_{0,1}$ depends only on the potential barrier parameters (barrier height and electron mass in the barrier) and has a non-zero value even at $m_A/m_B \to 0$. Applicability region of the obtained expansion is limited by very small μ values, at which $1/\tilde{A} = \mu a/B \ll 1$ may be assumed as small in the GBC applicability region for the ground state $B/a < B_{0,1}(\mu)/a$.

Now consider the deviation of the ground state energy $E_{0,1}$ from $E_{0,1}^\infty = E_q$ near $\mu = 1$ for high potential barriers $U/E_q \geq 1$. By expanding the left-hand side of equation (16) in small $1 - E_{0,1}/E_q$ and using smallness $\tilde{A} \ll 1$, we obtain

$$\frac{E_{0,1}}{E_q} \approx \frac{1}{\left(\tilde{A}\left[\tilde{A}+1\right]+1\right)^2} \Rightarrow E_{0,1} \approx \frac{\hbar^2\pi^2}{2m_A a^2\left[1+\sqrt{\frac{\hbar^2 m_B}{2m_A^2 U a^2}}+\frac{\hbar^2 m_B}{2m_A^2 U a^2}\right]^2}. \qquad (19)$$

Comparison of dependences $E_{0,1}/E_q$ on μ and U/E_q analytically calculated using expressions (18) and (19) with dependences obtained numerically with SBC and GBC is shown in Figure 6. It is shown that asymptotic expression (18) for $\mu \to 0$ the better describes the energy dependence on μ the lower the relative barrier height U/E_q. In case of high potential barrier $U/E_q = 20$, it is only applicable at $\mu < 0.005$. On the contrary, expression (19) is applicable to high potential barriers. For example, for $U/E_q = 20$, expression (19) satisfactorily describes the energy dependence on μ in a wide range of $0.03 < \mu \leq 1$ values.

Find the connection between A introduced by us into (7) with a_c introduced in [32] within the eight-band Kane model. By neglecting the dependence of the effective electron mass inside NC on the energy we obtain $a_c = -Am_B/m_0$. Using the experimental estimate of $a_c = -0.06$ nm for CdSe nanocrystals from [32,33] and assuming $m_B = m_0$, the potential barrier height may be estimated as $U \approx 10$ eV. It should be noted that, when the potential barrier height U and effective electron mass m_B outside NC are known, GBC (7) with surface parameter A or GBC for the eight-band Kane model with $a_c = -Am_B/m_0$ make it possible to find the electron state spectrum and wave functions inside NC. However, for the shell formed by organic ligands [12], the potential barrier height and effective mass are not always known. In this case, a_c shall be treated as a parameter characterizing the surface properties and supplementing the set of known parameters of a bulk semiconductor. a_c may be determined by comparison with experimental data, for example, as in [32,33].

It should be noted that the GBC surface parameter in the described model is always positive: $A = B > 0$ and $a_c < 0$. In such case, the GBC spectrum, like the SBC spectrum, does not contain surface Tamm states with energy in the band gap [16,32]. Such states may be obtained in the finite potential barrier model with addition of $2\alpha R_B/\hbar^2$ to the right-hand side of the second condition in SBC (6). Such BC describes the presence of zero-radius attractive potential in the form of $-\alpha\delta(r-a)$ at the heteroboundary [36,37]. A short-range potential may occur, for example, in transition from a multiband to one-band effective mass method [38] and when considering a narrow transition interface layer between layers A and B, where concepts of effective mass

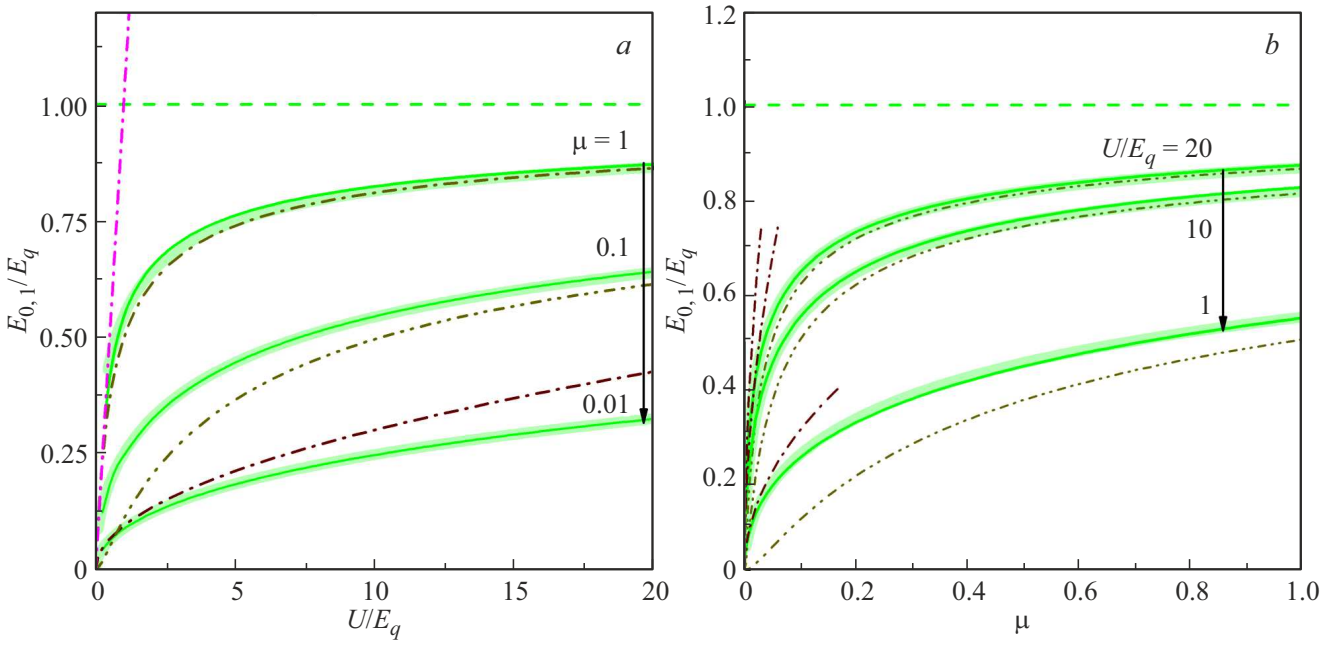

Figure 6. Dependences of the dimensionless ground state energy $E_{0,1}/E_q$ (a) on the potential barrier height U/E_q at three different μ, and (b) on μ for three different U/E_q. Calculations using SBC (solid lines), GBC (light thick lines), asymptotic expressions (18) (brown dot-and-dash line) and (19) (dot-dot-and-dash line) are shown. Pink dot-and-dash line in pane (a) shows the bound state existence region boundary; dashed lines correspond to $E_{0,1}^{\infty}$.

and envelope wave function are not defined [39]. α defines the short-range interface potential power, attractive ($\alpha > 0$) or repulsive ($\alpha < 0$). In case of attractive potential, interface Tamm states with band gap energy may exist. Such states are not discussed in this article.

According to the calculations and analytical study, considerable difference in the effective electron masses inside and outside the semiconductor NC typical for dielectric environment results in reduction of the electron size quantization levels. On the other hand, the effect of the dielectric constant difference inside a semiconductor and in the surrounding matrix, for example, in an organic ligand shell, is a feature of semiconductor NC in the dielectric medium that was not considered by us when determining the electron spectrum [12]. This difference results in strengthening of the Coulomb interaction between the carriers and to an increase in the level energy as a result of electric field penetration beyond NC even in case of infinite potential barrier [40–42]. Whilst consideration of the dielectric constant difference in the image charge method results in self-interaction electron potential going to infinity with a decrease in the distance to the NC surface. This, in turn, requires potential regularization in case of finite potential barrier for the electron [3,43,44]. Estimates obtained in this article for the relative length of wave function tunneling to the barrier B/a, at which the energy spectrum may be described with GBC, provide approximate assessment of the surface layer thickness where self-interaction potential regularization is necessary.

Possible experimental manifestations of the impact of the effective electron mass difference on the energy spectrum and wave functions are discussed below. In spherical NC, effects caused by the dielectric constant difference compensate each other and do not influence the exciton optical absorption energy. Therefore, even when the additional electron self-interaction energy corresponding to repulsion from the charge image is comparable with a decrease in the level energy caused by the effective mass difference, the last effect will influence the optical transition energy. In addition, the effective mass difference influences the difference of energies of symmetry levelss and p that may be determined by comparing single-photon and two-photon absorption spectra. When the electron mass outside NC increases, the probability of finding an electron on the surface also increases. This shall result in strengthening of electron/surface interaction, including an increase in the exchange interaction constant with dangling bonds with incomplete surface passivation and shall be manifested in the effects caused by the surface-induced magnetism.

6. Conclusion

Spherical semiconductor nanocrystals in dielectric medium or vacuum discussed in this article. It is shown that the high potential barrier at the semiconductor/dielectric interface may be treated as an impenetrable barrier with non-zero wave function at the nanocrystal surface. General boundary conditions with a surface parameter that explicitly

depends on the potential barrier and effective electron mass in the dielectric medium are established herein. The applicability region of general boundary conditions was defined, i. e. the potential barrier and nanocrystal parameter region where consistent description of energy spectrum and wave functions for four lower electron size quantization levels is possible. The influence of the electron mass in the dielectric medium on the energy spectrum and wave functions of electrons localized in NC was analyzed and possible experimental observation of such influence was discussed.

The developed method of determining the GBC and surface parameter applicability region is general and may be extended to the eight-band effective mass model taking into account the complex valence band structure. Such generalization is required to apply our impermeable NC surface model to a wider range of semiconductor materials. The question about the connection between the GBC parameter in the impenetrable surface model and the general BC parameters for the finite potential barrier remains open. The latter make it possible to consider the surface properties additional to the barrier height and effective mass beyond the barrier and to describe possible presence of surface Tamm states.

Appendix

1A. Equations for energy spectrum

With SBC:

$$\tan(k_0 a) = \frac{k_0 a}{1-\mu(1+\varkappa_0 a)} \equiv F_0(k_0 a, \varkappa_0 a, \mu),$$

$$\tan(k_1 a) = \frac{k_1 a}{1+\frac{k_1^2 a^2(\varkappa_1 a+1)}{\mu a^2 \varkappa_1^2 + 2(\varkappa_1 a+1)(\mu-1)}} \equiv F_1(k_1 a, \varkappa_1 a, \mu),$$

$$\tan(k_2 a) = \frac{k_2 a}{1-\frac{k_2^2 a^2}{3}\left[1+\frac{k_2^2 a^2}{9-k_2^2 a^2-3\mu\left(3+\frac{\varkappa_2^2 a^2(\varkappa_2 a+1)}{\varkappa_2^2 a^2+3\varkappa_2 a+3}\right)}\right]}$$

$$\equiv F_2(k_2 a, \varkappa_2 a, \mu). \quad \text{(A1)}$$

With GBC:

$$\tan(k_0 a) = \frac{k_0 a}{1-\frac{1}{\tilde{A}}} \equiv f_0(k_0 a, \tilde{A}),$$

$$\tan(k_1 a) = \frac{k_1 a}{1-\frac{k_1^2 a^2}{2-\frac{1}{\tilde{A}}}} \equiv f_1(k_1 a, \tilde{A}),$$

$$\tan(k_2 a) = \frac{k_2 a}{\left[1-\frac{k_2^2 a^2}{3-\frac{k_2^2 a^2}{3-\frac{1}{\tilde{A}}}}\right]} \equiv f_2(k_1 a, \tilde{A}). \quad \text{(A2)}$$

Limiting transition:

$$\lim_{\tilde{A}\to+\infty} f_0(k_1 a, \tilde{A}) = k_0 a,$$

$$\lim_{\tilde{A}\to+\infty} f_1(k_1 a, \tilde{A}) = \frac{k_1 a}{1-\frac{k_1^2 a^2}{2}},$$

$$\lim_{\tilde{A}\to+\infty} f_2(k_1 a, \tilde{A}) = \frac{k_2 a}{1-\frac{k_2^2 a^2}{3}\left[1+\frac{k_2^2 a^2}{9-k_2^2 a^2}\right]}. \quad \text{(A3)}$$

2A. Equations for critical power of spherical quantum well

Expression for $w_{0,n}$ will be written as

$$w_{0,n}\cot(w_{0,n}) = 1-\mu \equiv W_0(\mu). \quad \text{(A4)}$$

At $\mu = 1$, the electron localization occurs when $w_{0,n} = \pi(n-1/2)$.

Expression for $w_{1,n}$ will be written as

$$w_{1,n}\cot(w_{1,n}) = \frac{w_{1,n}^2 + 2(\mu-1)}{2(\mu-1)}$$

$$= 1-\frac{w_{1,n}^2}{2(1-\mu)} \equiv W_1(\mu, w_{1,n}). \quad \text{(A5)}$$

At $\mu = 1$, the electron localization occurs when $w_{1,n} = \pi n$.

Expression for $w_{2,n}$ will be written as

$$w_{2,n}\cot(w_{2,n}) = 1-\frac{w_{2,n}^2}{3}\left[1+\frac{w_{2,n}^2}{9(1-\mu)-w_{2,n}^2}\right]$$

$$= 1-\frac{3w_{2,n}^2(1-\mu)}{9(1-\mu)-w_{2,n}^2} \equiv W_2(\mu, w_{2,n}). \quad \text{(A6)}$$

At $\mu = 1$, equation (A6) coincides with the equation for spherical Bessel function roots j_1.

Acknowledgments

The authors are grateful to Al.L. Efros who has drawn their attention to the problem of investigation of the electron size quantization spectrum in nanocrystals taking into account the significant electron effective mass difference of a semiconductor and dielectric.

Funding

This study was supported by grant No. 23-12-00300 provided by the Russian Science Foundation, https://rscf.ru/en/project/23-12-00300/.

Conflict of interest

The authors declare that they have no conflict of interest.

References

[1] Al.L. Efros, L.E. Brus. ACS Nano **15**, *4*, 6192 (2021).
[2] A.I. Ekimov, A.A. Onushchenko. JETP Lett. **40**, *8*, 1136 (1984).
[3] L.E. Brus. J. Chem. Phys. **79**, *11*, 5566 (1983).
[4] Al.L. Efros, A.L. Efros. Sov. Phys. Semicond. **16**, *7*, 772 (1982).
[5] F.P.G. de Arquer, D.V. Talapin, V.I. Klimov, Y. Arakawa, M. Bayer, E.H. Sargent. Science **373**, *640*, 1 (2021)
[6] Y.-S. Park, J. Roh, B.T. Diroll, R.D. Schaller, V.I. Klimov. Nature Rev. Mater. **6**, *382* (2021).
[7] F. Meinardi, F. Bruni, S. Brovelli. Nature Rev. Mater. **2**, 17072 (2017).
[8] J.H. Olshansky, S.M. Harvey, M.L. Pennel, M.D. Krzyaniak, M.R. Wasielewski, R.D. Schaller. J. Am. Chem. Soc. **142**, *31*, 13590 (2020).
[9] C.R. Kagan, L.C. Bassett, C.B. Murray, S.M. Thompson. Chem. Rev. **121**, 3186 (2021).
[10] A.P. Alivisatos. Nature Biotechnology **22**, 47 (2004).
[11] A. Sukhanova, I. Nabiev. Critical Rev. Oncology/Hematology **68**, 39 (2008).
[12] C. Giansante. Chem. Eur. J. **27**, 14358 (2021).
[13] A.R. Khabibulin, Al.L. Efros, S.C. Erwin. Nanoscale **12**, 23028 (2020).
[14] J.W. Conley, C.B. Duke, G.D. Mahan, J.J. Tiemann. Phys. Rev. **150**, *2*, 466 (1966).
[15] D.J. Ben Daniel, C.B. Duke. Phys. Rev. **152**, *2*, 683 (1966).
[16] A. Rodina, A. Alekseev, Al.L. Efros, M. Rosen, B.K. Meyer. Phys. Rev. B **65**, *12*, 125302 (2002).
[17] N. Yahyaoui., N. Zeiri, P. Baser, M. Said, S. Saadaoui. Plasmonics **18**, 1 (2023).
[18] T. Ando, S. Mori. Surf. Sci. **113**, 124 (1982).
[19] G.T. Einevoll, L.J. Sham. Phys. Rev. B **49**, *15*, 10533 (1994).
[20] B. Laikhtman. Phys. Rev. B **46**, *8*, 4769 (1992).
[21] T. Ando, H. Akera. Phys. Rev. B **40**, *17*, 11619 (1989).
[22] Y. Fu, M. Willander, E.L. Ivchenko, A.A. Kiselev. Phys. Rev. B **47**, *20*, 13498 (1993).
[23] E.L. Ivchenko, A.Yu. Kaminski, U. Rossler. Phys. Rev. B **54**, *8*, 5852 (1996).
[24] A.B. Foreman. Phys. Rev. Lett. **81**, *2*, 425 (1998).
[25] V.L. Alperovich, D.M. Kazantsev, A.G. Zhuravlev, L.D. Shvartsman. Appl. Surf. Sci. **561**, 149987 (2021).
[26] D.M. Kazantsev, V.S. Khoroshilov, G.E. Shaibler, V.L. Alperovich. Physics of the Solid State **65**, *8*, 1219 (2023).
[27] D.B. Tran Thoai, Y.Z. Hu, S.W. Koch. Phys. Rev. B **42**, *17*, 11261 (1990).
[28] R. Vaxenburg, A. Rodina, A. Shabaev, E. Lifshitz, Al.L. Efros. Nano Lett. **15**, *3*, 2092 (2015).
[29] A. Shabaev, Al.L. Efros, A.L. Efros. Nano. Lett. **13**, 5454 (2013).
[30] L.S. Braginsky. Phys. Rev. B **60**, *20*, 13970 (1999).
[31] A. Rodina, Al.L. Efros. Nano Lett. **15**, *6*, 4214 (2015).
[32] A. Rodina, Al.L. Efros, A. Alekseev. Phys. Rev. B **67**, *15*, 155312 (2003).
[33] J. Gupta, D. Awshalom, Al.L. Efros, A. Rodina. Phys. Rev. B **66**, *12*, 125307 (2002).
[34] M. Abramowitz, I.A. Stegun. Handbook of Mathematical Functions with Formulas, Graphs, and Mathematical Tables. Dover Publications Inc, N.Y. (1992). 1046 p.
[35] J.K. Tomfohr, O.F. Sankey. Phys. Rev. B **65**, 245105 (2002).
[36] Yu.N. Demkov, V.N. Ostrovsky. Metod potentsialov nulevogo radiusa v atomnoy fizike. LGU, L. (1975), 240 p. (in Russian).
[37] V.M. Galitsky, B.M. Karnakov, V.I. Kogan. Zadachi po kvantovoy mekhanike. Nauka, M., (1992), 879 s. (in Russian).
[38] E.E. Takhtamirov, V.A. Volkov. JETP **89**, *5*, 1000 (1999).
[39] A. Rodina, A. Alekseev. Phys. Rev. B **73**, *11*, 115312 (2006).
[40] G.B. Grigoryan, A.V. Rodina, Al.L. Efros. Sov. Phys. Solid State **32**, *12*, 2037 (1990).
[41] N.A. Efremov, S.I. Pokutnii. Sov. Phys. Solid State **32**, *6*, 955 (1990). (in Russian).
[42] A.V. Rodina, Al.L. Efros. ZhETF **149**, *3*, 641 (2016).
[43] L. Banyai, P. Gilliot, Y.Z. Hu, S.W. Koch. Phys. Rev. B **45**, *24*, 14136 (1992).
[44] N.A. Efremov, S.I. Pokutnii. Sov. Phys. Solid State **32**, *10*, 1697 (1990). (in Russian).

Translated by E.Ilinskaya